Fast pulse-excited spin waves in yttrium iron garnet thin films

Mingzhong Wu, Boris A. Kalinikos,[a] Pavol Krivosik,[b] and Carl E. Patton
Department of Physics, Colorado State University, Fort Collins, Colorado 80523

(Received 28 June 2005; accepted 14 November 2005; published online 3 January 2006)

Fast pulse-driven spin-wave excitations in magnetic films have been studied experimentally and theoretically. The experiment was conducted on a low loss yttrium iron garnet thin-film strip with separate microstrip lines for excitation and detection. The theoretical analysis was based on the full spatio-temporal Fourier response of the input pulse/microstrip line configuration and the spin-wave dispersion for the film. The data and analysis provide a clear and precise picture of the manner in which the fast pulse-excited spin-wave signals are defined and controlled by the interplay of pulse rise time, excitation geometry, and spin-wave dispersion. The amplitude of the spin-wave wave packet associated with the leading or trailing edges of the drive decreases with the pulse rise time and the static magnetic field, and increases with the pulse amplitude. The spectral profile of the spin-wave excitation is highly asymmetric, with a steep lower-frequency edge and a gradual upper-frequency edge. The spectral bands are controllable; an increase in the static magnetic field pushes up the lower cutoff frequency, while an increase in the pulse rise time pushes down the higher cutoff frequency. © *2006 American Institute of Physics*. [DOI: 10.1063/1.2150592]

I. INTRODUCTION

Collective spin excitations in magnetic materials are often termed spin waves or, in certain limits, magnetostatic waves. Typically, the direct excitation of spin waves in a magnetic thin film is accomplished with a narrow strip line over the film and a cw or pulsed microwave input current applied to the line. Such strip line excitation methods for spin waves were developed and extensively studied in the 1970s and 1980s.[1–6] Such structures, moreover, have been widely used for studies of both linear and nonlinear spin waves[7,8] as well as spin-wave envelope solitons.[9,10] They have also been central to the development of a wide variety of microwave ferrite devices.[11] It is well established that in the case of linear excitations, the excited spin waves have the same frequency as the input microwave signal, while the spin-wave wave number is controlled by the spin-wave dispersion.

In principle, one can also replace the cw or pulsed microwave drive by a fast current pulse. The Fourier components of the fast rise time pulse serve the same function as direct microwave excitation in driving the spin waves. The faster the pulse rise time, the higher the frequency components in the Fourier makeup of the pulse. Fast current pulse techniques have been used since the 1960s to study magnetization switching processes in a variety of systems.[12,13] More recently, the demand for higher-density thin-film media and high-speed recording systems has led to a resurgence of interest in fast pulse driven switching.[14–25] In most of these studies, the switching was driven by a fast current pulse applied to a strip line placed over the film. The data generally showed an oscillatory decay in the dynamic magnetization and gave indications of (1) a dynamic reduction in the magnetization on a nanosecond time scale,[22] (2) an increase in the damping during the initial stages of the switching,[23,24] and (3) shifts in the oscillation frequency.[25] In spite of the fact that these were all pulse experiments, the three effects noted above all indicate a strong connection with spin-wave excitations.

Up until now, the only direct study of spin-wave excitations through the use of fast current pulse driven techniques has been by Covington *et al.*[26] These authors used a fast current pulse applied to one coplanar transmission line to excite a spin-wave pulse in a nickel-iron thin film and a second line placed 50 μm downstream to detect the propagating wave packet. While these authors were able to measure the decay of these propagating modes and obtain decay rates and damping parameters consistent with known values, the rapid decay rates for metals and the relatively short propagation distances precluded any quantitative analysis of the fast pulse generated modes.

This work reports experimental results and a full quantitative data analysis on fast pulse driven spin waves. There are three significant differences between this work and that in Ref. 26. First, the experiments are done on low loss yttrium iron garnet (YIG) films rather than on metallic films. The factor of 100 lower loss for YIG gives much longer propagation lengths for the spin-wave signals and allows for a more quantitative analysis of the spin-wave response. Second, the spin-wave response is analyzed in the frequency domain as well as in the time domain. Third, data as a function of pulse amplitude and rise time as well as the static field magnitude and direction allowed for a quantitative analysis of the various spatio-temporal control parameters on the fast pulse-excited spin-wave (FPESW) signals. Two microstrip line transducers were used for drive and detection. The data provide a clear and precise view of the interplay of spin-wave band structure, pulse rise time and amplitude, and

[a]Permanent address: St. Petersburg Electrotechnical University, 197376, St. Petersburg, Russia.
[b]On leave from the Faculty of Electrical Engineering and Information Technology, Slovak University of Technology, Bratislava, Slovakia.

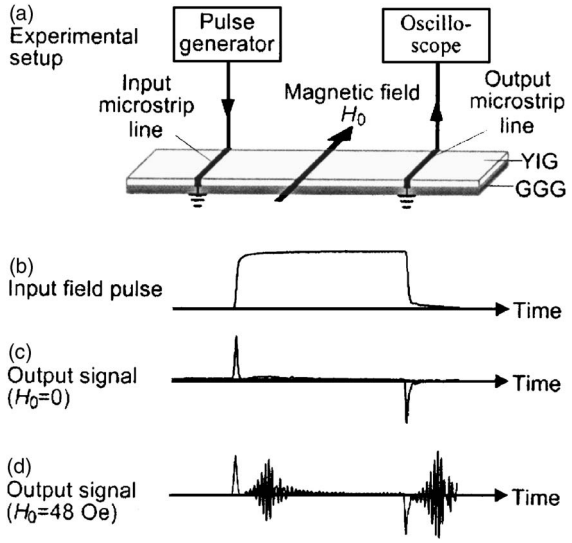

FIG. 1. Experimental setup and representative time-domain input and output signals for the fast pulse-excited spin-wave measurements. Graph (a) shows schematic diagram of the experimental setup. The yttrium iron garnet (YIG) film is on a gadolinium gallium garnet (GGG) substrate. A magnetic field H_0 is applied in the plane of and perpendicular to the long direction of the film strip. Graph (b) shows an input field pulse profile. Graphs (c) and (d) show the output signals for H_0=0 and H_0=48 Oe, respectively.

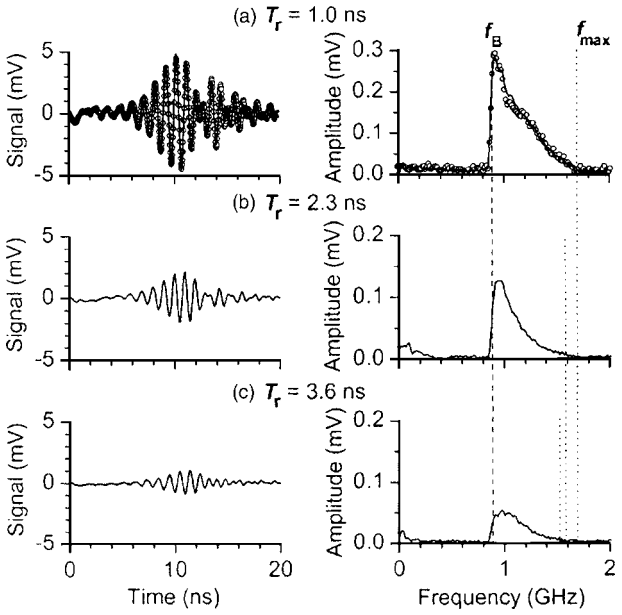

FIG. 2. Representative output wave forms and frequency spectra for three different input pulse rise times. The solid line traces are for an input pulse amplitude of 4.81 V. The data points in graph (a) are for a factor of 2.75 smaller drive and the points are scaled up by this same factor. The static field was 50 Oe. In the frequency spectrum graphs, the dashed line and the f_B label indicate the rise-time-independent low-frequency band-edge cutoff for the magnetostatic surface wave excitations, while the dotted lines and the f_{max} label indicate the rise-time-dependent upper-frequency limits.

excitation geometry to define and control FPESW signals. Theoretical analysis was also done based on the full spatio-temporal Fourier response of the input pulse/microstrip line configuration and the spin-wave dispersion for the film.

The organization of this paper is as follows: Section II describes the experimental setup and measurement specifics. Section III presents the experimental data on the FPESW signals as a function of pulse rise time, pulse amplitude, and static magnetic field. Section IV provides a theoretical analysis and numerical modeling for the FPESW processes.

II. EXPERIMENTAL SETUP AND MEASUREMENT SPECIFIC

Figure 1 shows the experimental setup and illustrative time-domain signals. Graph (a) shows a schematic diagram of the experimental setup. Graph (b) shows an input pulse profile. Graphs (c) and (d) show representative output signals. The experiment utilizes a long and narrow YIG film strip. Two microstrip line transducers are positioned over the film strip for the excitation and detection of spin-wave signals. The pulse generator provides fast current pulses to the input microstrip line. The oscilloscope is used to record the time-domain signals from the output microstrip line. The static magnetic field H_0 is applied in the plane of the film and perpendicular to the spin-wave propagation direction from input to output. This configuration corresponds to magnetostatic surface wave (MSSW) propagation.[7]

The YIG film strip was a 6.7-μm-thick, 2-mm-wide, 20-mm-long strip cut from a larger single-crystal film grown on a gadolinium gallium garnet substrate by standard liquid phase epitaxy technique. The film had unpinned surface spins and a nominal 10-GHz ferromagnetic resonance linewidth in the 1-Oe range. The microstrip lines were 50 μm wide and 2 mm long elements. For the data below, the separation between the microstrip lines was set to 2.15 mm. The drive consisted of 1–5 V, 20–600 ns wide pulses with rise times from 1 to 4 ns and a repetition rate of 10 kHz. A typical input pulse profile is shown in graph (b). All cited rise times denote the time taken for the input pulse to go from 10% to 90% of its amplitude.

For no applied field, the output signal consists of inductive rise time and fall time electromagnetic spikes only, as shown in graph (c). When a field is applied, follow-on MSSW wave packets similar to those shown in graph (d) are observed. The time delay between the spikes and the wave packets yields the group velocities for the MSSW signals. The time-domain wave forms below were obtained by subtracting the zero-field output signals from the signal traces for nonzero fields. The frequency spectra below were obtained through the fast Fourier transforms of the time-domain signals. There was no change in the MSSW wave-packet signals with input pulse width or repetition rate as long as the widths were maintained at a factor of 10 greater than the rise times. This shows that the rise and fall times are the critical input pulse parameters for the control of the spin-wave signals.

III. EXPERIMENTAL RESULTS AND DISCUSSIONS

Figures 2 and 3 show sequences of signal voltage versus time traces and frequency spectra for the FPESW wave packets. The Fig. 2 data are for a fixed static field of 50 Oe and a change in the pulse rise time T_r from 1.0 ns in (a) to 3.6 ns in (c). The Fig. 3 data are for a fixed rise time of 1.4 ns and a change in static field from 40 Oe in (a) to 80 Oe in (c). Graph (d) in Fig. 3 shows the integrated power, or the full

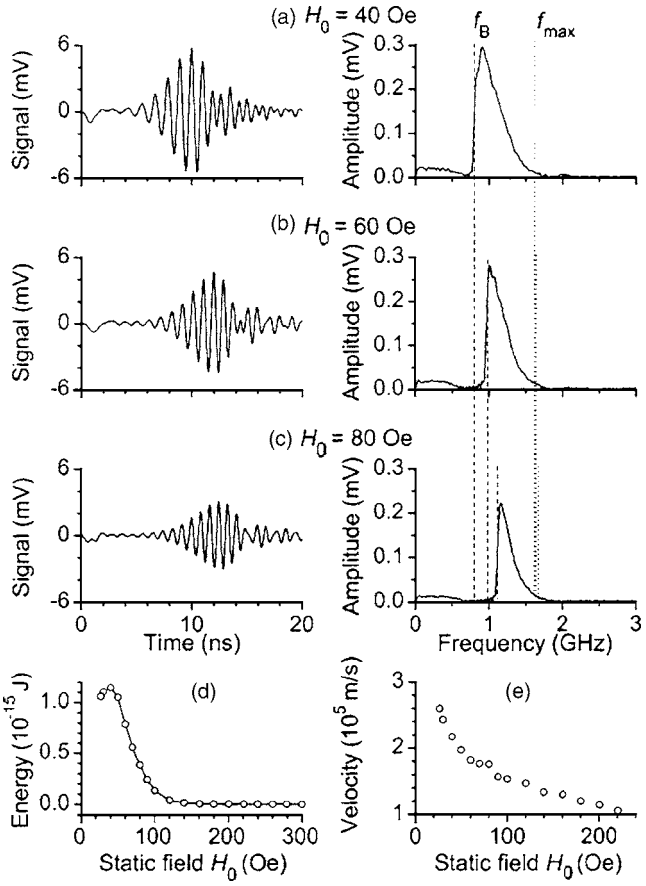

FIG. 3. The graphs in (a)–(c) show representative output wave forms and frequency spectra for three different values of the static field H_0, as indicated. The pulse amplitude and rise time were 5.13 V and 1.4 ns, respectively. In the frequency spectrum graphs, the dashed lines and f_B label indicate the field-dependent low-frequency band-edge cutoff for the magnetostatic surface wave excitations and the dotted line and f_{max} label indicate the field-independent upper-frequency limit. Graphs (d) and (e) show the integrated power and group velocity of the wave packets, respectively, as a function of static field for a pulse of the same amplitude and rise time as for graphs (a)–(c).

pulse energy for static fields from 25 to 300 Oe. Graph (e) shows the observed pulse velocity versus field from 25 to 220 Oe. In the frequency spectrum (FS) graphs, the dashed line and the f_B label indicate the low-frequency band-edge cutoff for the excitations, while the dotted lines and the f_{max} label indicate the upper-frequency limits.

These data demonstrate the quantitative connections that are possible for pulse-excited spin waves. The key is in the juxtaposition of the evolving frequency spectra and the time traces for the data shown. The increase in rise time from (a) to (c) in Fig. 2 pushes down frequency spectrum profile upper limit f_{max}. The increase in field from (a) to (c) in Fig. 3 pushes up the lower-frequency band edge f_B. While the pulse evolution is not particularly clear from the time traces, the frequency spectra give the full picture.

Consider the details: the solid line time traces in Fig. 2 were obtained for 4.81 V input pulse amplitudes. The empty circle data points in graph (a) were for pulses with smaller amplitude by a factor of 2.75, and the points have been scaled up by the same factor. The near perfect match between the line and point data in graph (a) clearly shows that the response is linear. As one goes from short to long rise times, one sees that the only apparent change in the FPESW wave packets is the expected drop in amplitude.

The FS profiles in Fig. 2 show, rather spectacularly, the real changes that take place for these FPESW wave packets. The main effect is that the upper-frequency limit decreases as the rise time increases. The vertical dotted lines with the f_{max} label delineate this limit change, from about 1.69 GHz in graph (a) to 1.52 GHz in graph (c). This change is due to a shift to lower frequencies in the Fourier makeup of the drive that excites these modes as the rise time is increased. Because the FS profiles show a gradual tail off at high frequency, the indicated f_{max} points here (and in Fig. 3) are taken at a level of 5% of peak amplitude. Notice that the sharp lower cutoff of the frequency spectra does not change. This cutoff corresponds to the field-defined MSSW low-frequency band edge at frequency f_B.

Figure 3 shows the effect of a change in static field at fixed pulse rise time on the FPESW wave packet and the corresponding frequency spectra. The pulse rise time was set at 1.4 ns. While there is some change in the shape and amplitude of the wave packets in graphs (a)–(c) with field, these changes are much more evident from the FS profiles. These spectra show clearly how the low-frequency cutoff point at f_B shifts up with field. The dashed lines show the theoretical band-edge frequency[7]

$$f_B = \frac{1}{2\pi}|\gamma|\sqrt{H_0(H_0 + 4\pi M_s)}, \tag{1}$$

where γ is the gyromagnetic ratio, taken at the free-electron value of -1.76×10^7 rad Oe^{-1} s^{-1}, and $4\pi M_s$ is the YIG saturation induction, taken at 1750 G. The field H_0 was adjusted upward by 8 Oe for the f_B determinations, as an empirical accommodation for the magnetocrystalline anisotropy in the (111) film. As the rise time was fixed, the change in the upper-frequency cutoff f_{max} is insignificant as shown in Fig. 3.

The (d) and (e) graphs in Fig. 3 show further manifestations of the field-tuned FPESW response. Graph (d) shows the integrated pulse power, or pulse energy, at the output transducer, obtained as the full time integral of $|V(t)|^2/R$, where $V(t)$ is the signal voltage and R is the 50-Ω oscilloscope load resistance. The precipitous falloff in the pulse energy for fields above 100 Oe marks the full collapse of the spectra as the f_B band edge moves into the rise time defined upper limit frequency f_{max}. The small falloff for fields below 40 Oe or so is due to the unsaturated magnetization state of the YIG film. Graph (e) shows the average speed of the wave packet as a function of static field. This group velocity decreases with increasing field and is in accordance with the changes in the MSSW dispersion curve with field.

The FPESW responses were also checked in two other ways. First, the linear response condition was tested by changing the transducer separation and checking that the drop in signal tracked the expected exponential decay. Second, the in-plane field direction was rotated away from the perpendicular-to-strip MSSW configuration and the change in the frequency spectra was correlated with the known change in the spin-wave dispersion. Such rotation serves to

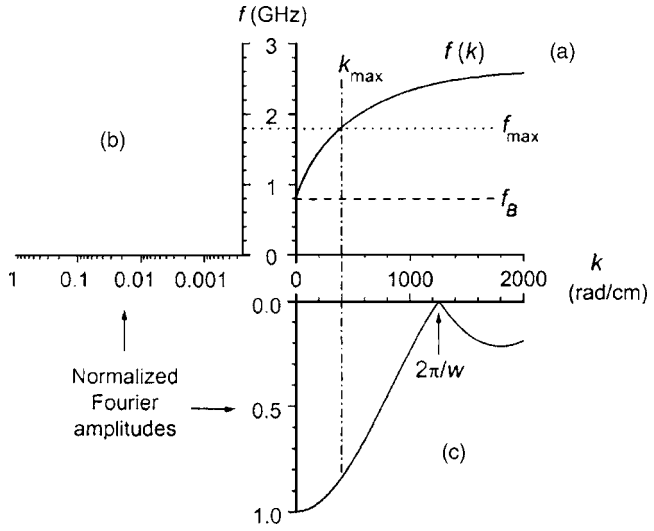

FIG. 4. Graph (a) shows a typical MSSW dispersion curve of frequency f vs wave number k for the same conditions as in Fig. 3(a). The shaded portion extends from the MSSW band-edge point at $f=f_B$ to an upper cutoff point at $f=f_{\max}$ related to the tail of the temporal Fourier response in (b). Graph (b) shows the normalized temporal Fourier amplitude response vs f for an input pulse with an exponential rise time of 0.64 ns. Graph (c) shows the normalized spatial Fourier amplitude response vs k for an input transducer width w of 50 μm. The vertical dashed-dotted line from graph (a) to graph (c) shows the cutoff wave number $k_{\max}$ that corresponds to the cutoff frequency $f_{\max}$.

collapse the MSSW band as the angle between the static field and the propagation direction is rotated away from 90°. The frequency spectra showed profiles that narrowed as expected. The rotation left the f_B band edge unchanged and caused the gradual upper cutoff at $f_{\max}$ to move down in frequency.

IV. THEORETICAL ANALYSIS

The remainder of the presentation is concerned with companion theoretical Fourier spectrum analyses and computed FPESW responses for comparison with the experimental data.

Figure 4 shows the approach. Graph (a) shows a typical MSSW dispersion curve of frequency f versus wave number k, based on the parameters for the experimental data in Fig. 3(a). The dispersion relation $f(k)$ is given by[7]

$$f(k)=\frac{|\gamma|}{2\pi}\sqrt{H_0(H_0+4\pi M_s)+(4\pi M_s)^2\left(\frac{1-e^{-2kd}}{4}\right)}, \quad (2)$$

where d is the film thickness. The heavily shaded portion of the $f(k)$ response extends from the MSSW band-edge point at $f=f_B$ to an upper cutoff point at $f=f_{\max}$ related to the tail of the temporal Fourier response in graph (b). Graph (b) shows the envelope of the normalized temporal Fourier amplitude response for an input pulse with exponential leading and trailing edges. A pulse profile with exponential leading and trailing edges practically fits the input pulse used in the experiment. The exponential rise (and falling) time is 0.64 ns. This value was chosen to match the experimental leading edge profile with a 10%–90% rise time of 1.4 ns. This graph is juxtaposed against graph (a) with a common frequency axis. Graph (c) shows the normalized spatial Fourier amplitude response for the input transducer with a width w of 50 μm. Such a response has the form[7]

$$A(k)=\sin\left(\frac{kw}{2}\right)\frac{2}{kw}. \quad (3)$$

Graph (c) is juxtaposed to graph (a) with a common wave-number axis. For reference, the cutoff wave number $k_{\max}$ that corresponds to the upper-frequency limit $f_{\max}$ is shown by the vertical dashed-dotted line from graph (a) to graph (c).

These diagrams help quantify the band-edge effects found experimentally. The lower cutoff frequency f_B is controlled by the bottom limit of the MSSW band at $k=0$. An increase in the magnetic field H_0 pushes up the cutoff frequency f_B. The upper-frequency limit $f_{\max}$ derives from the tail of the temporal Fourier-transform response. An increase in the rise time pushes down the upper-frequency limit $f_{\max}$. The signal level within the active band is determined by the projections of both the temporal and spatial Fourier responses on the dispersion curve and the small changes in group velocity as one moves from the lower cutoff f_B to the upper cutoff $f_{\max}$. These connections lead to the strong asymmetry of the FPESW spectra, sharp low-frequency band edges, and gradual high-frequency band edges, as shown in the FS graphs in Figs. 2 and 3. The spatial response in graph (c) produces no cutoff effect for the experimental parameters used here because the condition $2\pi/w > k_{\max}$ is satisfied.

Spatio-temporal Fourier and MSSW dispersion curves of the sort in Fig. 4, but for the full range of fields, field angles, and rise times in the experiments, were used to compute directly the dynamic magnetization response and full FPESW output profiles and frequency spectra for comparison with the experimental data. The starting point for this procedure is outlined in Ref. 27. There are three steps. One first uses Fourier responses like those in Fig. 4, in combination with the torque equation of motion and Maxwell's equations in the magnetostatic limit, to compute the dynamic magnetization spatio-temporal $\mathbf{m}_0(f,k)$ amplitudes at the input. One then allows these signals to propagate from the input to the output with a k-dependent group velocity $v_g(k)=2\pi\partial f(k)/\partial k$ and spatial decay rate $\eta/v_g(k)$, where η is the intrinsic relaxation rate obtained from separate decay measurements with cw microwave input signals. The dynamic response at the output transducer, $\mathbf{m}_L(f,k)$, where L is the transducer separation, is then back transformed and converted to an output voltage signal. It is also important to include a small gap spacing between the film and the transducers in the computation.

Figure 5 shows representative results in normalized form. The solid curves in all graphs show the computed responses for a static field of $H_0=48$ Oe and a rise time of 1.4 ns. The gap spacing between the film and the transducers was set at 30 μm to obtain the best match with experiment. Graphs (a) and (b) show time-domain wave forms and graph (c) shows the temporal Fourier transform of the wave form in graph (b). For reference, the dotted curve in graph (a) shows the shape of the input current pulse profile used in the computations, which has exponential leading and trailing edges. The empty circles in graphs (b) and (c) show experimental data for the static field of 40 Oe and a pulse rise time of 1.4 ns.

The results in Fig. 5 show a good correlation between

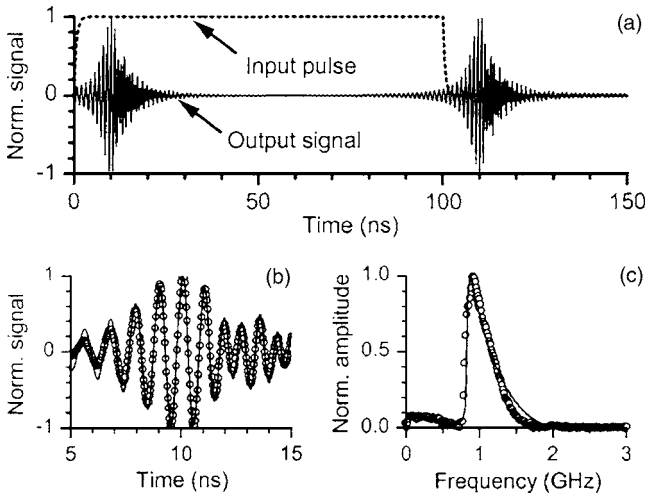

FIG. 5. Graph (a) shows the full computed output signal voltage (solid curve) and the input current pulse profile (dotted curve) used in the computations. The solid curves and empty circles in graphs (b) and (c) show computed and experimental normalized output voltage wave packets and frequency spectra for the fast pulse-excited spin-wave signals. The computed results are derived from parameters as in Fig. 4. The experimental data match those used for Fig. 3(a).

the computation and the experiment. The wave form in graph (a) shows two wave packets which correspond to the rise time and falling time excited spin-wave packets. In graphs (b) and (c), there is a good agreement between the computed and measured time-domain wave packets and frequency spectra. Similar agreement was found for the full range of pulse rise times, pulse amplitudes, and static magnetic fields used for the experiments.

V. SUMMARY AND CONCLUSIONS

This paper reports on a comprehensive set of measurements and analyses of fast pulse-excited spin waves in low loss yttrium iron garnet thin films. The experiment was conducted on a long and narrow YIG film strip with well-separated microstrip transducers placed over the strip for the excitation and detection of the spin-wave signals. The theoretical analysis was done based on the full spatio-temporal Fourier response of the input pulse/microstrip line configuration and the spin-wave dispersion for the film. The measured and computed data provide a clear and precise view on how the fast pulse-excited spin-wave signals are defined and controlled by the interplay of pulse rise time, excitation geometry, and spin-wave dispersion.

Two wave packets corresponding to the rise and fall edges of the input current pulse are excited. The amplitude of the spin-wave excitation decreases with the pulse rise time and the static field, and increases with the pulse amplitude. The spectral profile of the spin-wave excitation is highly asymmetric, with a steep lower-frequency edge and a gradual upper-frequency edge. The spectral bands are field and rise time controllable. An increase in the static magnetic field pushes up the lower cutoff frequency, while an increase in the pulse rise time pushes down the higher cutoff frequency.

These results show that (1) spin-wave excitations can be generated in fast current pulse experiments in a straightforward and controlled manner, and (2) the spatio-temporal response of these signals can be analyzed in terms of basic Fourier response and spin-wave dispersion considerations. While the measurements and analyses were made on the YIG thin films with microstrip lines for excitation and detection, the conclusions are general and applicable to other magnetic systems.

ACKNOWLEDGMENTS

This work was supported in part by the National Science Foundation (Grant No. DMR-0108797), the U. S. Army Research Office (Grant Nos. DAAD19-02-1-0197 and W911NF-04-1-0247), the Information Storage Industry Consortium (INSIC) Ultra High Density Recording (EHDR) program, and the Russian Foundation for Basic Research (Grant No. 05-02-17714). Dr. Pavel Kabos and Dr. Igor Kalinichenko, Nan Mo, and Kevin R. Smith are acknowledged for helpful discussions.

[1] A. K. Ganguly and D. C. Webb, IEEE Trans. Microwave Theory Tech. **23**, 998 (1975).
[2] A. K. Ganguly, D. C. Webb, and C. Banks, IEEE Trans. Microwave Theory Tech. **26**, 444 (1978).
[3] J. C. Sethares, IEEE Trans. Microwave Theory Tech. **27**, 902 (1979).
[4] P. R. Emtage, J. Appl. Phys. **49**, 4475 (1978).
[5] A. Kalinikos, Sov. Phys. J. **24**, 719 (1981).
[6] I. J. Weinberg and J. C. Sethares, IEEE Trans. Microwave Theory Tech. **32**, 463 (1984).
[7] D. Stancil, *Theory of Magnetostatic Waves* (Springer-Verlag, New York, 1993).
[8] P. Kabos and V. S. Stalmachov, *Magnetostatic Waves and Their Applications* (Chapman & Hall, London, 1994).
[9] B. A. Kalinikos, N. G. Kovshikov, and A. N. Slavin, Sov. Phys. JETP **67**, 303 (1988).
[10] S. O. Demokritov, A. A. Serga, V. E. Demidov, B. Hillebrands, M. P. Kostylev, and B. A. Kalinikos, Nature (London) **426**, 159 (2003).
[11] J. D. Adam, L. E. Davis, G. F. Dionne, and E. F. Schloemann, IEEE Trans. Microwave Theory Tech. **50**, 721 (2002).
[12] W. Dietrich and W. E. Proebster, J. Appl. Phys. **31**, 281S (1960).
[13] P. Wolf, J. Appl. Phys. **32**, 95S (1961).
[14] C. H. Back, R. Allenspach, W. Weber, S. S. P. Parkin, D. Weller, E. L. Garwin, and H. C. Siegmann, Science **285**, 864 (1999).
[15] T. J. Silva, C. S. Lee, T. M. Crawford, and C. T. Rogers, J. Appl. Phys. **85**, 7849 (1999).
[16] M. Bauer, R. Lopusnik, J. Fassbender, and B. Hillebrands, Appl. Phys. Lett. **76**, 2758 (2000).
[17] B. C. Choi, M. Belov, W. K. Hiebert, G. E. Ballentine, and M. R. Freeman, Phys. Rev. Lett. **86**, 728 (2001).
[18] W. Bailey, P. Kabos, F. Mancoff, and S. Russek, IEEE Trans. Magn. **37**, 1749 (2001).
[19] Th. Gerrits, H. A. M. van den Berg, J. Hohlfeld, L. Bar, and Th. Rasing, Nature (London) **418**, 509 (2002).
[20] B. Hillebrands and J. Fassbender, Nature (London) **418**, 493 (2002).
[21] H. W. Schmacher, C. Chappert, P. Crozat, R. C. Sousa, P. P. Freitas, J. Miltat, J. Fassbender, and B. Hillebrands, Phys. Rev. Lett. **90**, 017201 (2003).
[22] T. J. Silva, P. Kabos, and M. R. Pufall, Appl. Phys. Lett. **81**, 2205 (2002).
[23] J. P. Nibarger, R. Lopusnik, and T. J. Silva, Appl. Phys. Lett. **82**, 2112 (2003).
[24] L. Lagae, R. Wirix-Speetjens, W. Eyckmans, W. Hiebert, and J. De Boeck, 9th Joint MMM/Intermag Conference (Anaheim, California, 2004).
[25] M. L. Schneider, A. B. Kos, and T. J. Silva, Appl. Phys. Lett. **85**, 254 (2004).
[26] M. Covington, T. M. Crawford, and G. J. Parker, Phys. Rev. Lett. **89**, 237202 (2002).
[27] B. A. Kalinikos and A. N. Slavin, Acta Phys. Pol. A **A75**, 541 (1989).